CHAPTER 5
TEST & MEASUREMENT OF THE APD

The performance of the lidar system is ultimately determined by the intrinsic performance of the APD photodiode. Test and measurement of the prime parameters of the APD photodiode are presented in a progressive approach, beginning with the description of an efficient way of illumination of the active are of the device. The measurements performed are: quantum efficiency, *M-V or gain-bias characteristics,* mean responsivity, local variations of both the multiplication factor and the responsivity, dark current components and excess noise factor. In addition, the natural flow of the text gives a brief outline of the measurement procedure, test set-ups used and very often, an extended error analysis that focus on the measurement confidence.

1. ILLUMINATION OF THE ACTIVE AREA

1.1 Measurement wavelength and correction factors

All the APD measurements have been carried out with light of a wavelength of *830 nm,* because this was the wavelength of the available laser. This will be named the reference wavelength λ_{ref}.

To correct the results that will be presented later to the lidar operating wavelengths *(532 nm* and *1064 nm)*, correction factors are derived next. These correction factors have been obtained from the responsivity curve of the device in the data sheet, and they are the main error source when performing wavelength conversions. These are the responsivity values read at the operating point specified by the manufacturer (i.e. at $V_R = 375\ V$):

- $R_i(\lambda_{ref}) = 30.84 \pm 0.54$ A/W at $\lambda_{ref} = 830$ nm
- $R_i(\lambda_1) = 66.83 \pm 1.20$ A/W at $\lambda_1 = 532$ nm
- $R_i(\lambda_2) = 33.64 \pm 0.58$ A/W at $\lambda_2 = 1064$ nm

If the correction factor for the responsivity at wavelength λ is defined as

$$C_R(\lambda) = \frac{R_i(\lambda)}{R_i(\lambda_{ref})} \tag{1}$$

the correction factors at the lidar wavelengths become

- $C_R(532) = 0.4615$
- $C_R(1064) = 0.5034$

Likewise, correction factors for the quantum efficiency can easily be derived. From the definition of intrinsic responsivity given in Chap.3, Sect.2.1, which is reproduced next

$$R_{io} = \eta \frac{q\lambda}{hc} \quad \rightarrow \quad R_i = R_{io}M \tag{2}$$

the correction factor for the quantum efficiency may be defined as

$$C_\eta(\lambda) = \frac{\eta(\lambda)}{\eta(\lambda_{ref})} \tag{3}$$

The manufacturer does not specify any curve for the quantum efficiency, so the correction coefficients must be obtained indirectly from those of the responsivity. By merging eqs.(1),(2) and (3), they can be related in the following way

$$C_\eta(\lambda) = C_R(\lambda)\frac{\lambda_{ref}}{\lambda} \tag{4}$$

At the wavelengths of interest, they become

- $C_\eta(532) = 0.7199$
- $C_\eta(1064) = 0.3926$

1.2 Illumination of the active area

The first idea was to illuminate the whole active area of the photodiode with a big spot coming out from the laser diode. When the spot is big enough, there is an area with nearly uniform distribution in the centre of the spot. Computations show that when the measurements is done with a light spot whose width is $w \geq 40$ *mm* (at *50 %* intensity), the absolute error in the measurement is about *0.08 %,* which is negligible in front of the accuracy of the *ML 9002A Anritsu optical power meter* (5 %) used for the power measurements. Under these circumstances, the optical power falling onto the active area of the APD can be calculated by the ratio of the active areas of the optical power sensor and the APD. This method was first used and it turned out that the active area of the APD had to be larger than the specified one. Later, examination of the active area under the microscope revealed the truth of that affirmation. Yet, since the area of the APD could not precisely be measured, an illumination method whose accuracy no longer relied on the diameter of the active area was sought. Thus, the uncertainty parameter was avoided.

The second measurement method consisted in *illuminating only a small point of the active area.* That gave the best results since it enabled to measure even local variations of the multiplication factor and of the responsivity. However, the main advantage from this method comes from the fact that when a small spot is used, its energy can entirely be measured with the optical power meter, and the same energy falls on the active area of the APD. The only source of error of this method is introduced by the optical power meter rather than by the area of the APD.

Finally, good results were achieved by projecting the image of the end of a *50-μm* optical fibre onto the active area of the APD (Fig.1). In the set-up, the laser *(20-mW power)* was adjusted to infinity (i.e. light rays leaving the laser were parallel). The laser beam could be attenuated by using an adjustable optical attenuator. Behind it, a lens *(f = 50 mm)* focused the beam on the end of *50-μm* fibre. Even though the coupling at this point was not very good, *a well defined light source appeared at the other end of the fibre.*

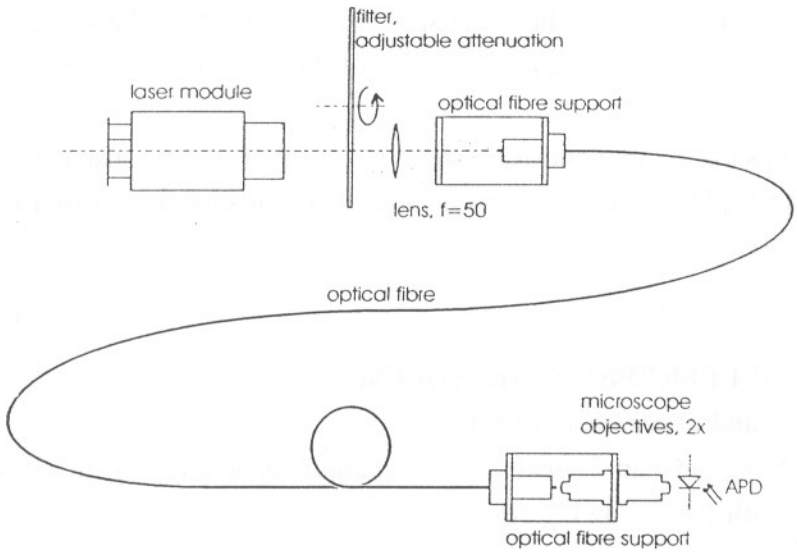

Fig.1 Optical system to illuminate the APD with a small light spot.

This light source has to be projected onto the active area of the APD. A system formed by two identical microscope eyepieces with magnification factor *(x20)* performs the projection. To focus the system, an indirect method has to be followed since monitoring the adjustment with an *IR-sensitive camera,* results impossible.

Fig.2 depicts the procedure steps:

First, the terminal of the fibre is placed in the focus of the first objective. This is controlled with the eye. When the fibre's end is seen focused, light rays leaving the eyepiece are parallel (Fig.2a). The second step is to repeat this adjustment with the second eyepiece and the APD. Once this is done, a bundle of parallel lights rays entering the eyepiece from the eye's side will be focused on the active area (Fig.2b). Finally, these two parts are placed close to each other on a common optical axis (Fig.2c).

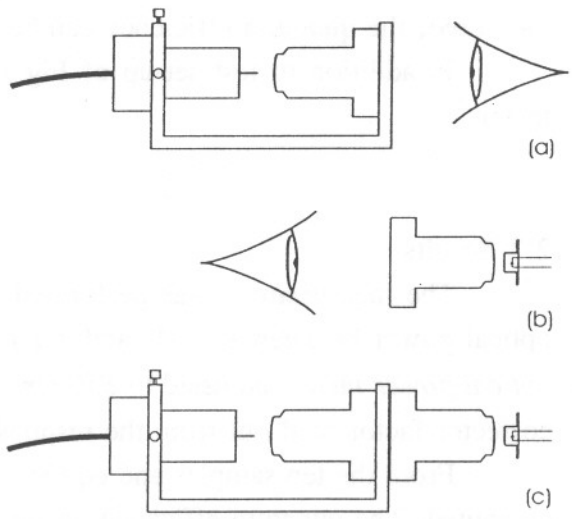

Fig.2 Focusing procedure steps.

	Image size	Pixel size	Spot size
Horizontal	6 pixels	13.75 μm	75 $\pm$ 7 μm
Vertical	5 pixels	16 μm	72 $\pm$ 8 μm

Tab.1 Spot size in the CCD display.

Additionally, so as to check the spot size, the APD was replaced by an *IR-sensitive CCD-camera.* By counting pixels, the image of the light spot could be estimated as shown in Tab.1.

To measure the photocurrent, the lidar receiver was not used. Instead, the voltage drop across a simple load resistor was measured. By this means, calibration of the receiver was not necessary.

2. QUANTUM EFFICIENCY MEASUREMENT

2.1 Procedure and experimental set-up

According to Chap.3, Sect.2.1, the quantum efficiency, η, in a device without gain is calculated with the following formula

$$\eta = \frac{I_{ph}}{P_{opt}} \frac{1.24 \cdot 10^{-6}}{\lambda} \tag{5}$$

where

I_{ph} is the photocurrent,
P_{opt} is the incident optical power and,
λ is the wavelength of the incident light.

So, when the active area is illuminated with a well defined amount of monochromatic light of known wavelength *(830 nm)* and the output photocurrent is measured, the quantum efficiency can be calculated (continuous light was used).

In addition to test set-up of Fig.1, an *HP 3457A Multimeter* worked as ampere meter.

2.2 Results

The measurement was performed ten times with ten different adjustments of the optical power between *8.4 μW* and *1.1 mW.* The power was measured with the *Anritsu optical power meter,* adjusted to *850 nm.* Subsequently, the values were corrected with a corrector factor read out from the responsivity curve of the instrument.

From the ten samples and eq.(5), ten values for the quantum efficiency have been computed. The quantum efficiency is derived form the slope of the line

$$I_{ph} = P_{opt} \bar{\eta} \frac{\lambda}{1.24 \cdot 10^{-6}} \tag{6}$$

with $\bar{\eta}$, the expectation value calculated from linear regression of nine of the ten samples. One has been left out since it lays too far outside from the range of the others.

The graphical proceduce is illustrated in Fig.3, which yields:

$$\eta = 76.40 \pm 0.5\ \%$$

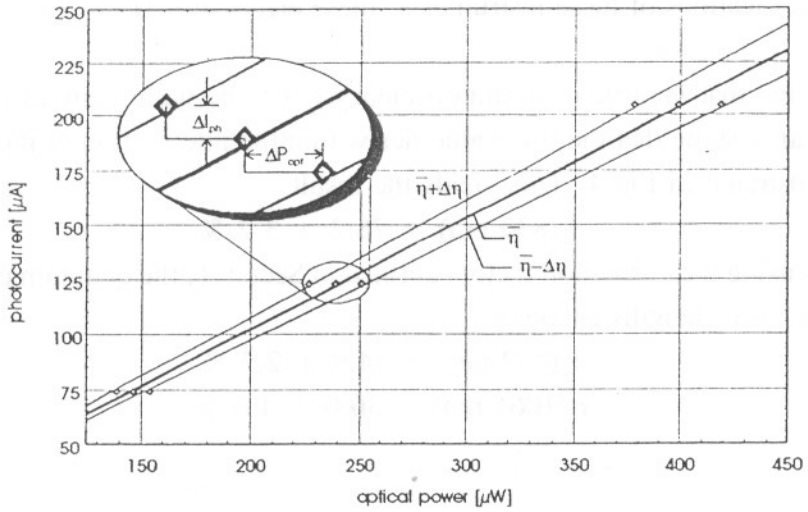

Fig.3 Graphical method to estimate quantum efficieny and systematic errors.

2.3 Extended error analysis

The error given above is calculated form the standard deviation of the results for the quantum efficiency. This assumes that the only error sources are statistical fluctuations in the measurement of the optical power and photocurrent.

However, there is another source of error that must be taken into account: the so-called *systematic error.* The characteristic of the systematic error is that however hard the measurement is repeated under the same conditions, the same difference between observed value and real value falsifies the measurement result [161].

The mathematical analysis of the effect of the systematic errors of the measured values on the quantum efficiency, yields the equation

$$\Delta\eta = \frac{\partial\eta}{\partial I_{ph}}\Delta I_{ph} + \frac{\partial\eta}{\partial P_{opt}}\Delta P_{opt} \qquad (7)$$

to calculate the error range for any of the nine samples separately. In the equation above, ΔI_{ph} and ΔP_{opt} (see Fig.3) are the systematic errors of the *HP 3457A* multimeter and of the *Anritsu handy optical power meter,* respectively. These systematic errors arise from the process when the instrument transforms the measured analog value to a digital number.

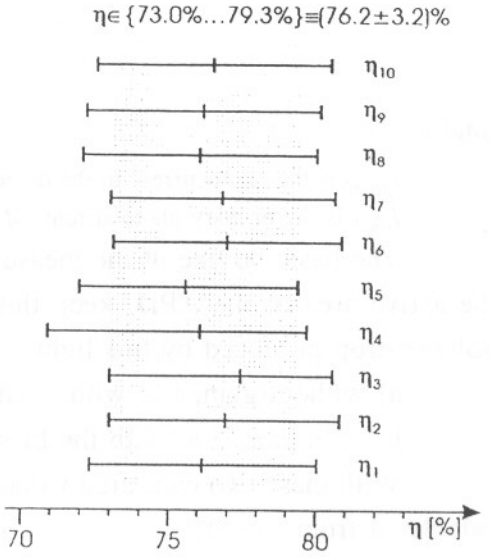

Fig.4 Uncertainty arrays in the computation of quantum efficiency η.

From the specifications of these instruments, these errors are $\Delta I_{ph} = 10.4\ nA$ and $\Delta P_{opt} = 5\% \cdot P_{opt}$.

Knowing that the true quantum efficiency has to be within any of these nine error arrays, one can assume that the true value lies within the intersection of these arrays. This method is illustrated in Fig.4. This yields the result

$$\eta(830\ \text{nm}) = 76.2 \pm 3.2\ \%$$

Now, using the correction factors defined in Sect.1.1, the quantum efficiency at the lidar operating wavelengths becomes:

$$\eta(532\ \text{nm}) = 54.9 \pm 2.3\ \%$$
$$\eta(1064\ \text{nm}) = 30.0 \pm 1.3\ \%$$

3. MULTIPLICATION FACTOR MEASUREMENT

The gain or multiplication factor, *M,* determines the amplification factor for the primary photocurrent produced by the APD by incoming light. This gain is a function of the reverse polarization of the device, V_R. The goal of this section is to obtain the *M-V characteristics* of the APD for a specified ambient temperature.

3.1 Procedure and experimental set-up

From eq.(2), the multiplication factor can be determined from the ratio of responsivities with and without gain. This is to say, that the multiplication factor can be determined as

$$M = \frac{I_{ph,M}}{I_{ph,1}} \tag{8}$$

where

$I_{ph,M}$ is the photocurrent in the device with gain M and,
$I_{ph,1}$ is the primary photocurrent $(M=1)$.

The basic outline of the measurement procedure can be given like this: illuminate the active area of the APD, keep this illumination constant and measure the current or voltage drop produced by this light:

a) without gain, i.e. with a sufficiently low bias $(V_R = -15\ V)$ and,

b) with gain, i.e. with the bias voltage V_R.

With these two measured values, the gain for the biased photodiode can directly be calculated from eq.(8).

Basically, the test set-up was the same as for the measurement of the quantum efficiency (Fig.1). The only difference between the two arrangements is that now, modulated light is used to enable detection with a lock-in amplifier.

Minimum and maximum applied polarizations were *15 V* and *420 V,* respectively.

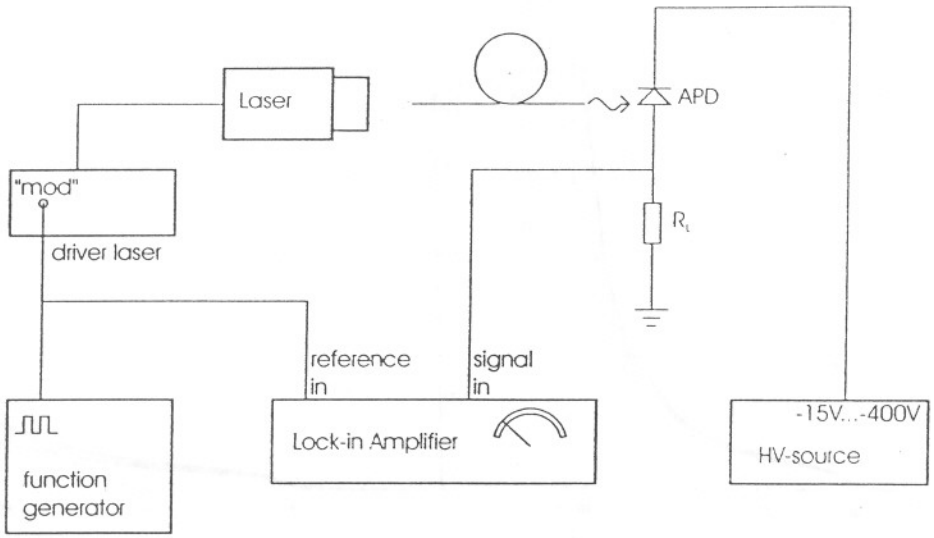

Fig.5 Experimental set-up to measure the M-V characteristics of the APD.

When the maximum voltage is applied, caution must be taken not to exceed maximum power dissipation of the device, which is *100 mW*. This limit is expressed as

$$P = V_R I_{ph} \; ; \qquad P_{\max} = 100 mW \tag{9}$$

where P is the power dissipated by the APD and P_{max} is the maximum limit given by the manufacturer. According to Chap.3, Sect.2.1 and eq.(2), the photocurrent is

$$I_{ph} = \eta \frac{q\lambda}{hc} P_{opt} M \tag{10}$$

When the maximum polarization voltage *(420 V)* is applied, the gain should be *120 (value given in the data sheet)* and then, from eq.(9), the maximum optical power calculates to $P_{op,max} \approx 4\ \mu W$. With *4* μW of optical power, the expected current limits should vary between *2* μA and *240* μA, when the gain varied between *1 (no gain)* and *120 (typ)*.

Yet, it is worth noting that the specification of the typical gain of an APD is always given at a specified ambient temperature. A reasonable conclusion is that that given ambient temperature must also be the junction temperature at the time of measurement. With the heat developed with *4* μW of optical power, measurement of the typical gain would be impossible. There are two possibilities to provide ambient temperature conditions in the junction: cooling the APD or applying an optical power level low enough to maintain heating of the junction negligible.

Finally, extremely low-light levels and a lock-in amplifier (Brookdeal Electronics Ltd., Mod.9503 SC [129]) were used to measure the very small electrical signal produced. The experimental set-up is shown in Fig.5. The APD was loaded with a *1622*-Ω metal film resistor and a programmable high-voltage source *(HVS) (Stanford Research Systems, Inc. Mod.PS350)* was used.

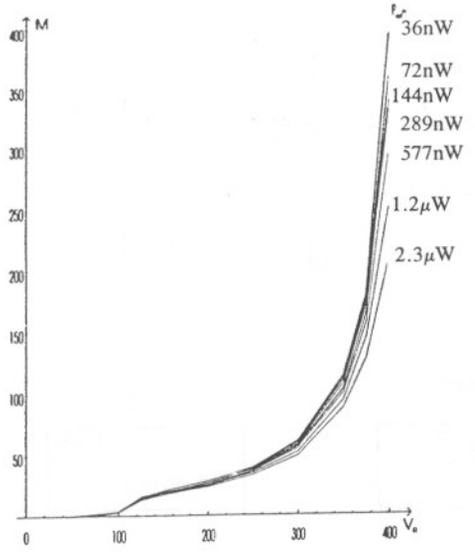

Fig.6 Multiplication factor (APD mounted in receiver case).

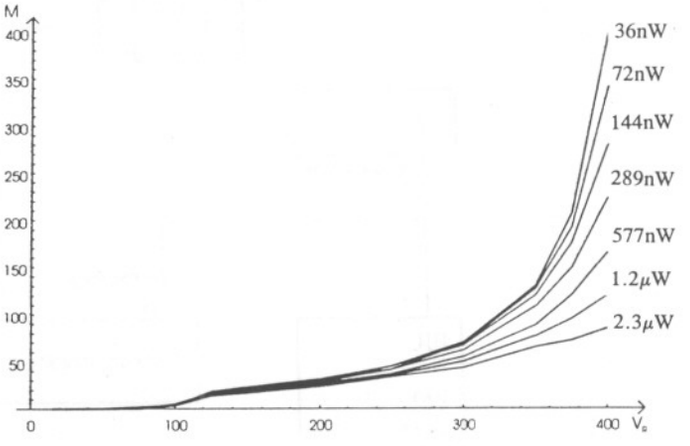

Fig.7 Multiplication factor (APD isolated from receiver case).

3.2 Results

Fig.6 shows ***M-V characteristics*** for the optical powers levels applied. The set of optical powers used in the measurement are labeled in the same figure.

This group of curves is not what was expected. According to specs, the measurements for different optical powers should yield only one curve and this curve should pass $M=120$ at the operation voltage $V_R= 375$ V.

It seems obvious that the multiplication factor decreases due to an increase of temperature, caused by the consumption of electrical energy at the P-N junction.

To verify this theory, the experiment was repeated with a significant change. The first time the *M-V characteristic* was measured (Fig.6), the APD was mounted in the receiver box with mechanical contact between the metal case of the APD and the metal of the receiver case (aluminium). This contact provided cooling to the APD. The second time, the experiment was repeated but with the APD isolated, i.e. without mechanical contact with the receiver case. In this experimental set-up, the variation between the curves for different optical power was much greater than those of the first experiment. Fig.7 shows the graphic yielded by this second experiment. From the comparison of Fig.7 with Fig.6, two very important conclusions can be reached:

1.- *The variation between the curves for different optical power are much larger without the heat sink. From this, one can conclude that the variations between the different curves result from different junction temperatures.*

2.- *The curve for the lowest applied optical power* (36 nW) *is practically the same in the measurement with or without heat sink. From this, one can conclude that there is no significant variation in temperature between the two experiments for this optical power.*

For the second point, two possible explanations exist: The power consumption due to the photocurrent may be negligible at all, then the junction temperature may be assumed to be the same as ambient temperature. Or, the power consumption due to the photocurrent may be negligible in comparison to the power consumption due to the dark bulk current. In this case, no statement about the junction temperature can be made.

To be able to make a statement about the influence of the dark bulk current on the heating of the *P-N junction,* let us compare the electrical power dissipated in the junction due to the photocurrent with the power dissipated due to the dark current. This calculation is done best for the operating point, at $V_R = 375V$.

a) *Dissipation due to the incident optical power.* In the experiment without heat sink and with an optical power of *36 nW,* the voltage drop at the load resistor *(1622 Ω)* was *6.2 mV rms,* which results in a dissipation of *1.4 mW* of electric power.

b) *Dissipation due to the dark current* (see definition in Chap.3, Sect.2.1). In another experiment (Sect.6.1) the surface and bulk dark current components were measured, yielding $I_{ds} \approx 13.8\ nA$ and $I_{db} \approx 6\ pA$. According to our measurement, at $V_R = 375\ V$, the multiplication factor was $M = 180$. At that bias, the dark current would be $I_{ds} + M I_{db} = 15\ nA$. (eq.(25), Chap.3). Since that current contributes to heating the *P-N junction,* this consumption would be $15\ nA \times 375\ V = 5.6\ \mu W$.

Note that the noise current spectral density $(i_n = 2\ pA\ Hz^{-1/2})$ does not contribute to dissipation since it is a zero mean process and the diode is reversed biased at a constant potential V_R.

Since the dark current consumption (b) is negligible in front of the energy dissipated due to the photocurrent, one can conclude that in the measurement of the M-V characteristic, the junction temperature was equal to the ambient temperature of 23 °C, when measured with the lowest applied power of 36 nW.

A logarithmic plot of the multiplication factor, *M,* of the APD as a function of the polarization voltage V_R, with the *P-N junction* at ambient temperature *(23 °C)* is shown in Fig.8. The measurement was done with the incident power of *36 nW.* The measured points, which are connected by straight lines in Fig.8, are listed in Tab.2. An interpolation procedure of this table has been included in *link-budget* software.

V_R	15	30	50	75	100	125	150	200	250	300	350	375	400
M	1	1.1	1.2	1.6	3.7	16	21	28	40	61	113	180	393
ϵ_M	0	4.7%	4.6%	4.4%	4.0%	4.9%	3.9%	4.6%	4.1%	4.7%	4.0%	5.0%	4.8%

Tab.2 Gain $M = f(V_R)$ at $T_A = 23°C$ and measurement error.

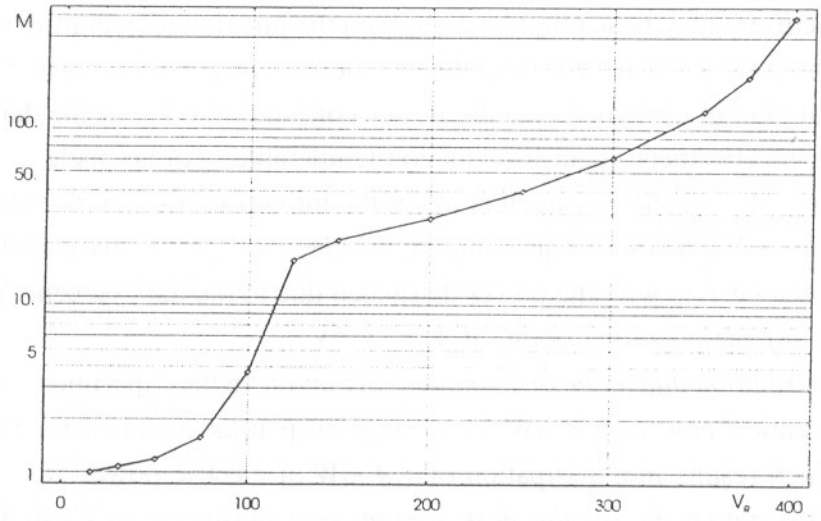

Fig.8 M-V characteristic of the APD with the p-n junction at T_A=23 °C.

The fact that for different optical powers, a family of *M-V characteristics* were obtained has some implications to the lidar project:

In the system configuration to scan the far range, the APD will be polarized with high voltages in order to produce a measurable signal from the reduced power that returns from large distances. To protect the data acquisition card in the PC from being overloaded at low ranges, the lidar receiver uses a disable feature controlled by the synchronization unit (see Chap.4). Yet, it must be warned that in the case of the analog receiver, this feature only disables the last amplification stage but not the APD. This means that the APD will still be exposed to the full optical power arriving from close distances and will produce the full, amplified photocurrent. The effect that such large photocurrent might play on the variation of the junction temperature (and therefore, on the multiplication factor) cannot be inferred from the experiments discussed but it seems sensible to assume that the effect will be negligible. This can be justified considering the low pulse repetition time of the lidar system *(100 ms or 10 Hz)* and the fact that the hot diffusion equation is ruled by diffusion times much larger that any lidar return signal. Thus considering a maximum lidar range of *12 km,* the lidar-return signal would last for *40 μs.*

3.3 Extended error analysis

The manufacturer of the lock-in amplifier, specifies the following accuracies [129]:

calibration accuracy: $\pm$ *3% and,*

meter accuracy: $\pm$ *2% of full-scale.*

Errors due to the calibration accuracy are of a constant percentage of the reading within the whole measurement range. Thus, they are systematic errors. Errors due to the limited meter accuracy are not repetitive in several measurements, they are statistic errors.

As it was done with eq.(7), the influence of the *statistical errors* on the multiplication factor can be computed by total differentiation of eq.(8), which yields

$$\epsilon_M = \frac{1}{M}\sqrt{\left(\frac{I_{ph,M}}{I_{ph,1}^2}\Delta I_{ph,1}\right)^2 + \left(\frac{\Delta I_{ph,M}}{I_{ph,1}}\right)^2}\cdot 100 \quad \% \tag{11}$$

The statistical error ϵ_M in the measurement at ambient temperature ($T_A = 23°C$, $P = 36\ nW$) is given in Tab.3.

The systematic error in the measurement is calculated with the formula

$$\Delta M_{sys} = \frac{\Delta I_{ph,M}}{I_{ph,1}} - \frac{I_{ph,M}}{I_{ph,1}^2}\Delta I_{ph,1} \tag{12}$$

With the lock-in amplifier accuracies given at the beginning of this section, $\Delta I_{ph,1} = 0.03 \cdot I_{ph,1}$ and $\Delta I_{ph,M} = 0.03 \cdot I_{ph,M}$, the systematic error is cancelled ($\Delta M_{sys} = 0$).

Measurement uncertainties are not the only reason for uncertainties of the value for M. A more important effect on the uncertainty of the multiplication factor of the APD at high bias voltages has the junction temperature and therefore, the incoming optical power.

During the experiment, the applied optical power varied between *36 nW* and *2.3 mW*. Seven different values of *M*, were obtained for every bias voltage. Tab.3 lists their mean and standard deviation.

V_R	15	30	50	75	100	125	150	200	250	300	350	375	400
$\overline{M}$	1	1.1	1.2	1.6	3.9	15.0	19.2	26.2	36.7	55.9	102	160	310
σ	0	0	0	0	0.2	0.9	1.2	1.7	2.5	4.3	9.1	18.7	64.2
ϵ_M	0	0.6%	1.6%	0.6%	5.0%	5.9%	6.2%	6.6%	6.8%	7.6%	8.9%	12%	21%

Tab.3 Mean multiplication factor, calculated from measurement values with different optical powers.

4. MEAN RESPONSIVITY COMPUTATION

The intrinsic responsivity can be calculated according to eq.(2) and the correction factors given in Sect.1 (eq.(1)). The following results are obtained:

- $R_{io}(830\ nm) = 512 \pm 26\ mA/W$
- $R_{io}(532\ nm) = R_{io}(830) \cdot C_R(532) = 236.5 \pm 12\ mA/V$
- $R_{io}(1064\ nm) = R_{io}(830) \cdot C_R(1064) = 257.9 \pm 13\ mA/V$

The total responsivity, R_i, can be computed from these values and the multiplication gain given in Tab.2 and Tab.3. For the typical multiplication gain $M = 120$, the current responsivities, R_i, are *7.98 % at* $\lambda = 532\ nm$ and *8.00 % at* $\lambda = 1064\ nm$ less that the ones specified by the manufacturer.

5. LOCAL VARIATIONS WITHIN THE ACTIVE AREA

If the responsivity shows local variations within the active area of the APD, then the photocurrent produced by a determined light power will also depend on the size of the light spot. Thus, it is important to know what are the local variations of the responsivity since they directly contribute to local variations of the multiplication factor.

5.1 Local variations of the responsivity

5.1.1 Procedure and test set-up

The responsivity, R_i is defined as the quotient of the photocurrent to the optical power:

$$R_i = \frac{I_{ph}}{P_{opt}} \tag{13}$$

Since the responsivity is the parameter most sensitive to error of the APD, a relative measurement is performed. As it was explained in Sect.3, the electrical signal produced by the APD is measured with the lock-in amplifier and the variation of the output signal of the APD due to changes of the light spot position on the active area is used to characterize the local variation of the responsivity. The measurement relies on the experimental set-up of Fig.1 and Fig.5. This set-up provides both convenient illumination of the active area with a small light spot and the possibility of obtaining accurate photocurrent measurements, both with and without avalanche gain.

Due to the time consuming measurements, the local variation of the responsivity was measured at two operation points, once with the APD in PIN mode (i.e. at $V_R = 15\ V$), and once at the working point specified by the manufacturer (i.e. at $V_R = 375\ V$). With these two bias voltages, measurements were performed on a grid of equidistant points covering the whole active area. An scheme of the measurement grid is given in Fig.9. The small circles are positions of the light spot, whose diameter were *75 μm,* approx.

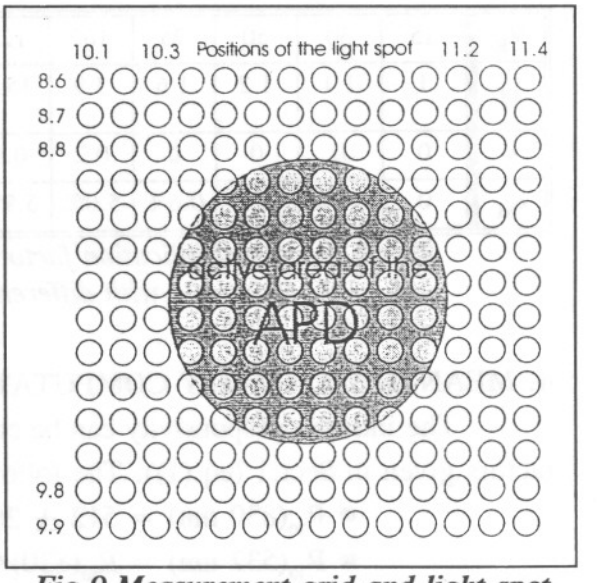

***Fig.9 Measurement grid and light spot positions in* mm.**

To define the size of the matrix of points of measurement, the lateral and top extremes of the matrix area were searched

by moving the APD with the positioning screws until the voltage reading was nearly zero. At these points, the APD position relative to the *0.0* mark of the positioners was noted down. From there, a matrix of *14x15 points with 100-μm spacing in both horizontal and vertical axis was set up*. Fig.15 shows a photograph of the set-up.

5.1.2 Results

Once the *210 positions of the matrix (14x15 points)* were measured for each polarization, the maximum was normalized to unity. Then, the whole matrix was multiplied by the responsivity figure at $V_R = 15\ V$, $\lambda = 830\ nm$, given in Sect.4.

Before having final results, some processing of the measurements was needed. First, an interpolation function searched the point of maximum responsivity in the measurement grid. Once the coordinates of the maximum were known, the coordinates of the system were made relative to it. In the new coordinate system, the responsivity was smoothed using a two-bidimensional interpolation function, $R_i(y,z)$, where y and z are the horizontal and vertical distances of the point (y,z) to the maximum. In Fig.10 and Fig.11, a three-dimentional plot of the interpolation function for the bias voltages $V_R = 15\ V$ and $V_R = 375\ V$ is shown. Values on the *y-axis* and *z-axis* are displayed in *μm*. Each square is *100x100 μm* in size.

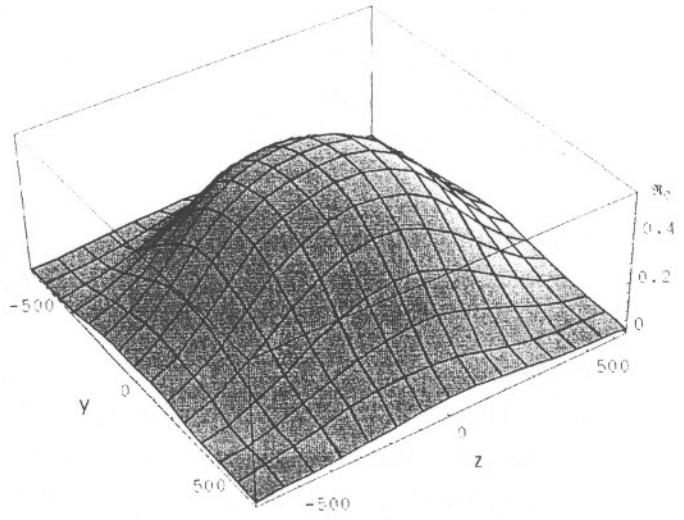

Fig.10 Local variation of the APD responsivity, $\mathbf{R_{io}}$ **(V_R=15 V).**

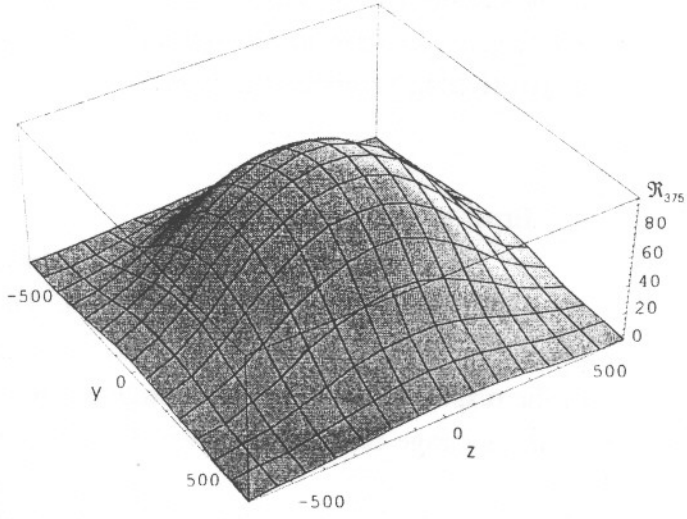

Fig.11 Local variation of the APD responsivity, $\mathbf{R_i}$ **(V_R=375 V).**

5.2 Local variations of the multiplication factor

With the two measurement matrices, another interesting computation can be done: by dividing the matrix of responsivity values measured at $V_R = 375\ V$ by the matrix of responsivities measured at $V_R = 15\ V$ (intrinsic responsivity or responsivity without gain), the matrix of local distribution of the multiplication factor, *M*, is obtained.

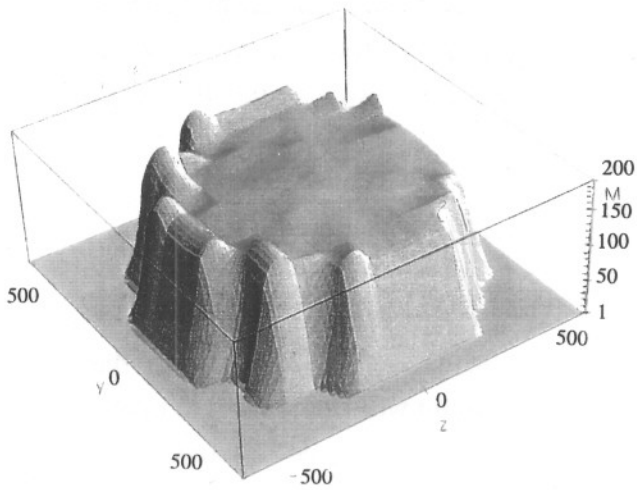

Fig.12 Local variation of the multiplication factor,* M, *over the active area of the APD.

In the plots of the local variation of the responsivity, it could be seen that some signal had been measured even when the light spot position had already left the active area. These values appeared due to measurement errors or perhaps due to some light of the image of the fibre that was not focused on the active area but was lost owing due to aberrations of the optical system. They had a large random component and led to partly very high results for the multiplication factors outside the active area. Because of that, these values had to be filtered.

Fig.12 shows the interpolation of the *M-matrix*. It turns out that the multiplication factor is nearly uniform over the active area. Only at the border there are some increases in the multiplication factor. They occur at positions where the light spot already leaves the active area. In these zones, the ratio of responsivities at the two voltages is very sensitive to positioning errors of the light spot.

5.3 Error analysis

The results shown are based on the hypothesis that the responsivity is uniform over the spot area, whose diameter is *75 μm*. This can perfectly be assumed, considering the small size of the light spot used. Yet, correction factors are needed when the measurement of the responsivity is done with larger light spots since then the responsivity measured will be the average responsivity over the spot area.

$$\overline{R_i}(\Delta S_{spot}) = \frac{\int_{\Delta S_{spot}} R_i(y,z)\,dy\,dz}{\Delta S_{spot}} \qquad (14)$$

6. DARK CURRENT COMPONENTS

In Sect.2.1 a measurement set-up was introduced to measure the quantum efficiency and, in particular, the output current of the APD directly with a precision ampere-meter *HP 3457A*. This set-up was also used to measure the total dark current, I_d, of the APD.

Based on Chap.3, Sect.2.1, the relation between total dark current and its components, surface dark current and bulk dark current, obeys the equation

$$I_d = I_{ds} + M \cdot I_{db} \tag{15}$$

Yet, measurement of the dark-current with an ampere-meter must take into account an extra component that increases with the bias voltage according to Ohm's law and which is due to the parasitic parallel resistance of the APD, R_p. Hence,

$$I_d(V_R) = I_{ds} + M(V_R) \cdot I_{db} + \frac{V_R}{R_p} \tag{16}$$

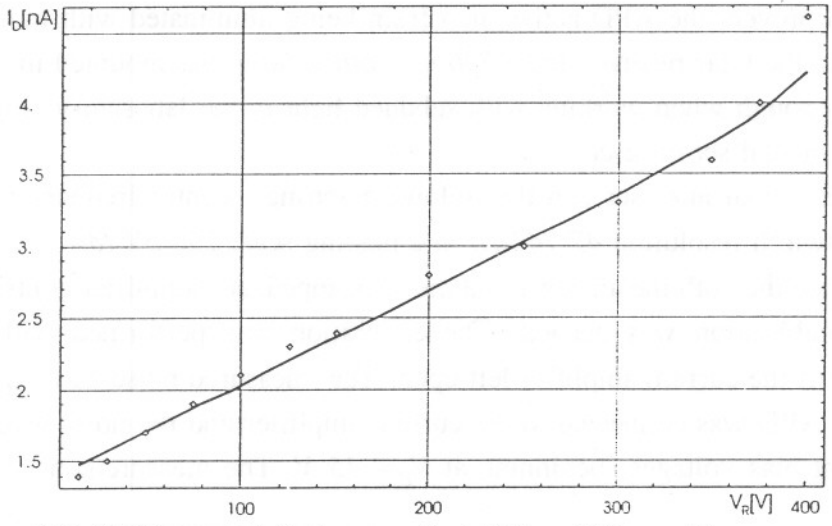

Fig.13 Measured dark current at different bias voltages.

Fig.13 shows the result of the dark current measurement for different bias voltages. For each bias voltage, the APD gain was computed according to Tab.2. To these values, the dark current function of eq.(16) was fitted with a mathematical program. The program yielded the sought-after parameters:

I_{ds} = 13.87 nA	I_{db} = 6.067 pA	R_p = 15.45 GΩ

Tab.4 Measured dark current component (eq.(16)).

7. NOISE SPECTRAL DENSITIES

7.1 Procedure and test set-up

For the measurement of noise spectral densities, a *Dynamic Signal Analyser, HP 3561A,* was available. However, analyser's inherent noise level was too high to carry out the measurement. Because of that, an optional transimpedance amplifier of the Brookdeal lock-in amplifier was used in front of it. This amplifier provided a stable transimpedance gain as high as 10^7 *V/A,* which lifted the APD signal to a detectable level.

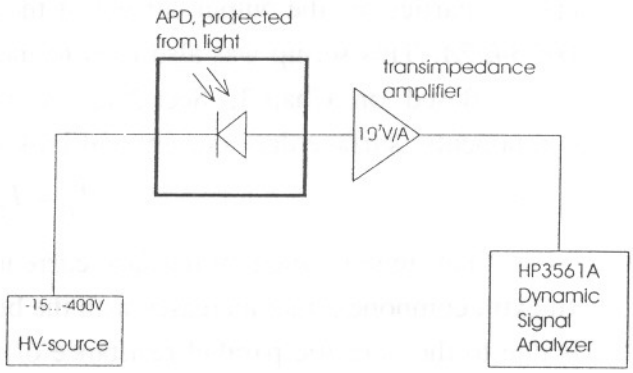

Fig.14 Test set-up to measure the noise generated by the APD.

To prevent the APD active area from being illuminated with light, the APD was mounted in the lidar receiver and a *830 nm optical filter* was mounted in the filter carrier. This was enough when working with subdued light in the laboratory. Fig.14 reproduces the experimental set-up used.

The signal analyser had the following settings: centre frequency *10 kHz,* span *5 kHz,* bandwidth resolution *47.742 Hz* and reading scale *250* pV^2/div.

Since the both the analyser and the transimpedance amplifier contribute to the total noise, a calibration was needed. The calibration was performed with the *current-in* connector of the current amplifier left open. The measured noise was $v_{offset}^2 = 73.88\ pV^2$. Then, the APD was connected to the current amplifier and the noise level was measured at different bias voltages, beginning at $V_R = 15\ V$. The measurement was repeated five times.

Finally, the average noise current spectral density is computed in three steps: First, the squared voltage spectral density is averaged over the five measurements, which gives $\overline{v_n^2}(V_R)$. Second the net squared noise voltage is computed by subtracting the noise offset and it is normalized to *1-Hz* bandwidth.

$$\overline{v_n^2}(V_R) = \frac{\overline{v_{read}^2} - v_{offset}^2}{BW} \tag{17}$$

And third, the average noise current spectral density is calculated as

$$\overline{i_n}(V_R) = \frac{\sqrt{\overline{v_n^2}(V_R)}}{G} \tag{18}$$

where G is the gain of the current amplifier (in the set-up, $G = 10^7$ *V/A).*

7.2 Results

Theoretically, the dark noise current spectral can be computed by (see Chap.3, Sect.2.1)

$$\sigma_{sh,d}^2 = \overline{i_n^2} = 2q[I_{ds} + F(M)M^2 I_{db}] \tag{19}$$

Note that in Chap.3 Sect.1, the noise current spectral density is denoted in terms of the dark shot variance, $\sigma_{sh,d}{}^2$.

Once the average noise current spectral density, $\overline{i_n^2}(V_R)$, is measured according to the procedure of Sect.7.1, eq.(20) can be solved for the excess-noise factor, F. This yields Tab.5.

V_R [V]	M	i_n [pA·Hz$^{-1/2}$]	F
15	1	0.159	$10.7 \cdot 10^3$
30	1.1	0.162	$9.3 \cdot 10^3$
50	1.2	0.154	$6.9 \cdot 10^3$
75	1.6	0.163	$4.5 \cdot 10^3$
100	3.7	0.165	$8.6 \cdot 10^2$
125	16	0.161	43.4
150	21	0.163	25.7
200	28	0.172	16.5
250	40	0.196	10.9
300	61	0.259	8.64
350	113	0.471	8.78
375	180	0.795	9.97
400	393	2.236	16.64
$i_{n,offset}$ = 0.124 pA·Hz$^{-1/2}$			

Tab.5 Measured noise current spectral density and excess-noise factor.

Theoretically, according to Chap.3, Sect.2.1, the excess-noise factor can be developed as

$$F(M) = kM + \left(2 - \frac{1}{M}\right)(1-k) \tag{20}$$

where k is the ionization ratio. Additionally, many manufacturers approximate F, using the empirical formula (see also Chap.3, Sect.2.5.2):

$$F(M) \approx M^x \tag{21}$$

Typical values of F at the working point of $V_R = 400\ V$ are about $F=10$, for a EG&G silicon reach-through structure [149], as is the case of our *EG&G C30954E* photodiode. The same reference assumes $k=0.02$ and $x=0.30$. Similar values can be found in reference [127].

From Tab.5, only excess-noise factors corresponding to bias voltages in the range $V_R \in [300, 400]\ V$ are meaningful. Note that for lower bias voltages, the excess-noise factor calculated is far from any physical meaning. Physically, the lower the gain, the lower the excess-noise. Below the range indicated, the equivalent input noise of the spectrum analyser becomes dominant and falsifies the measurements.

To compute the ionization ratio and the *x-factor,* current noise spectral density figures comparable to the equivalent current noise offset measured during the calibration step, have been discarded. The interval of useful data coincides with the interval of bias voltages between *300 V and 400 V,* where the excess-noise factor, follows and increasing trend, as it should be. Exponential regression over the four pairs *(M,F)* yielded the following factors:

- **k-factor** (ionization ratio) = **0.033**
- **x-factor** = **0.423**

Tab.6 compares these results with ref.[149]. For the detector type, *silicon reach-through structure,* which the case of our APD, the excess-noise factor has also been calculated for a non-typical gain of $M=400$. This helps comparison between referenced and measured values. From this comparison, it turns out that the measured values are something higher than the referenced ones.

In Ref.[123] an experimental set-up to measure the excess-noise factor of APDs is suggested. The set-up uses two lock-in amplifiers to reduce measurement errors. This procedure was not applied because only one lock-in amplifier was available.

DETECTOR TYPE	GAIN (M)	F	k-factor	x-factor
C30954E silicon reach-through structure (measurement)	400	16.64 *	0.033	0.423
Silicon reach-through structure	100 (typ) 400	4.0 10.0 *	0.02	0.30
Silicon (very-low-*k* structure)	200	2.4	0.002	0.17
Germanium	10	9.2	0.9	0.95
InGaAs	10	5.5	0.45	0.75

Tab.6 Typical and measured excess-noise factors from [149].

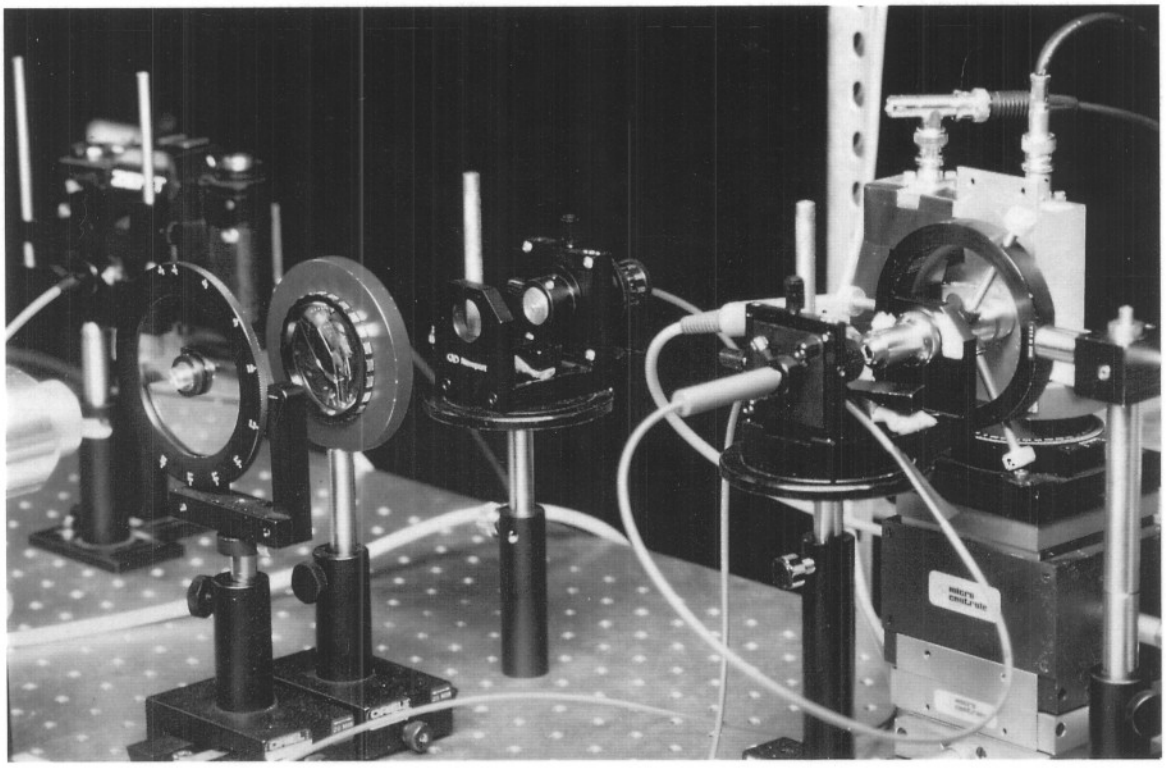

Fig.15 Test set-up to measure local variations using a small light spot.